The 2019 World Congress on
Advances in Structural Engineering and Mechanics (ASEM19)
Jeju Island, Korea, September 17 - 21, 2019

Natural Element Evaluation of SIFs in 2-D Isotropic Functionally Graded Materials

*Jin-Rae Cho[1)]

[1)] *Department of Naval Architecture and Ocean Engineering, Hongik University, Sejong 30016, Korea*
[1)] *jrcho@hongik.ac.kr*

ABSTRACT

This paper is concerned with the numerical evaluation of the stress intensity factors (SIFs) of 2-D isotropic functionally graded materials (FGMs) by the natural element method (more exactly, Petrov-Galerkin NEM). The spatial variation of elastic modulus in inhomogeneous FGMs is reflected into the modified interaction integral $\tilde{M}^{(1,2)}$. The local NEM grid near the crack tip is refined, and the strain and stress fields that were directly approximated by PG-NEM were enhanced and smoothened by the patch recovery technique. Numerical examples with the exponentially varying elastic modulus are taken to illustrate the proposed method. The stress intensity factors are parametrically evaluated with respect to the exponent index in the elastic modulus and the crack length, and those were compared with the other reported results. From the comparison with the analytical solutions, the prediction accuracy of the proposed method has been verified such that the maximum relative difference is less than 3%. In addition, it has been also confirmed that the proposed method is correlated satisfactorily with the J_k^* – integral using FEM and the modified interaction integral $\tilde{M}^{(1,2)}$ using EFGM.

1. INTRODUCTION

A functionally graded material (FGM) was introduced in the late 1980s to overcome the demerits of traditional layered heat-resisting composite materials (Apalak 2014). The thermal stress concentration at the layer interface, which was the most significant problem of layered heat-resisting composites, could be successfully reduced by inserting a graded layer between two different homogeneous material layers (Giannakopulos et al. 1995; Miyamoto et al. 2013). The thermo-mechanical behaviors of FGMs are influenced by the geometry, dimension, orientation and microstructure of constituent particles as well as the external loading and constraint. In particular, the structural failure of FGMs is dominated by micro-cracking because the microstructure is highly heterogeneous (Kawasaki and Watanabe 2002). In this context, the computation

of stress intensity factors and the crack propagation simulation have been an important research subject (Dolbow and Gosz 2002; Kim and Paulino 2002; Zhang et al. 2004; Tilbrook et al. 2007), in order to tailor FGMs which can be protected from the crack-driven failure.

One can employ traditional $J-$integral or interaction integrals for homogeneous materials. But, these standard integral methods provide path-dependent SIFs when applied to non-homogeneous materials. It is because the material properties vary point by point in non-homogeneous materials, but these standard integral methods cannot account for this spatial variation of material properties (Gu et al. 1999). The studies on the crack problems for non-homogeneous materials were initiated in the 1960~70s by assuming the spatial variation of the elastic modulus as an exponential function (Atkinson and List 1978; Dhaliwal and Singh 1978; Delale and Erdogan 1983). Gu et al. (1999) presented a simplified method for calculating the crack-tip field of FGMs using the equivalent domain integral technique. Anlas et al. (2000) numerically evaluated SIFs in FGMs by discretizing the material property variation and by assigning different homogeneous elastic properties to each element. Kim and Paulino (2002) evaluated the mixed-mode SIFs in FGMs using FEM analysis with three different approaches.

As an extension of our previous work (Cho and Lee 2006; Cho 2016), this paper intends to extend the Petrov-Galerkin natural element method (PG-NEM) to the calculation of SIFs of 2-D isotropic functionally graded materials. Differing from most grid point-based meshfree methods, PG-NEM is characterized by the accurate and effective implementation of the essential boundary conditions and the numerical integration. The spatial variation of the elastic modulus of FGMs is considered by the modified interaction integral $\tilde{M}^{(1,2)}$. The approximated strain and stress fields by NEM are enhanced by the recovery technique, and furthermore the near-tip NEM grid is locally refined. Numerical example with exponentially varying elastic modulus and external loading is taken. The calculated SIFs are compared with the other reported values in order to justify the numerical accuracy of the proposed method.

2. MODIFIED INTERACTION INTEGRAL $\tilde{M}^{(1,2)}$ FOR FGMs

Let us consider a 2-D linearly elastic and isotropic FGM shown in Fig. 1 with a crack inclined by α which occupies an open bounded domain $\Omega \in \Re^2$ with the boundary $\partial\Omega = \overline{\Gamma_D \cup \Gamma_N \cup \Gamma_c}$. Here, Γ_D denotes the displacement boundary, Γ_N the traction boundary, and $\Gamma_c = \overline{\Gamma_c^+ \cup \Gamma_c^-}$ the crack surface. FGMs are a representative inhomogeneous material such that the elastic modulus E and the Poison's ratio ν vary continuously on the material domain Ω. The material constants should be viewed as the effective ones in the macroscopic sense (Vel and Goupee 2010), because those are spatially discontinuous in the microscopic sense.

For mathematical description purpose, we use two Cartesian coordinate systems, $\{x,y\}$ for the 2-D linear elasticity problem and $\{x',y'\}$ for the stress intensity factor of angled crack respectively. Assuming the crack surface is traction-free and neglecting the body force $\boldsymbol{b}$, then the displacement field $\boldsymbol{u}(\boldsymbol{x})$ in the Cartesian coordinate system $\{x,y\}$ is governed by the static equilibrium

$$\nabla \cdot \boldsymbol{\sigma} = 0 \quad in \quad \Omega \tag{1}$$

with the displacement and traction boundary conditions

$$\boldsymbol{u} = \hat{\boldsymbol{u}} \quad on \quad \Gamma_D \tag{2}$$

$$\boldsymbol{\sigma} \cdot \boldsymbol{n} = \begin{cases} \hat{\boldsymbol{t}} & on \quad \Gamma_N \\ 0 & on \quad \Gamma_c^{\pm} \end{cases} \tag{3}$$

In which $\boldsymbol{\sigma}$ indicates the Cauchy stress and $\boldsymbol{n}$ the outward unit vector normal to $\partial\Omega$ and $\hat{\boldsymbol{t}}$ the surface force. By assuming small displacement and strains, the Cauchy strain $\boldsymbol{\varepsilon}$ is defined by the (3×2) gradient-like operator $\boldsymbol{L}$ such that

$$\varepsilon = \varepsilon(\boldsymbol{u}) = \boldsymbol{L}\boldsymbol{u} \tag{4}$$

Letting $\boldsymbol{D}$ be the constitutive tensor, the stresses and strains are constituted by

$$\boldsymbol{\sigma} = \boldsymbol{D} : \boldsymbol{\varepsilon} \tag{5}$$

Note that the displacement, strains and stresses are calculated based on the coordinate system $\{x, y\}$ and transformed into the coordinate system $\{x', y'\}$ using the chain rule and Mohr's circle.

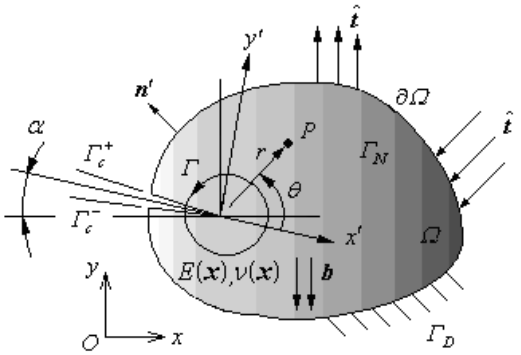

Fig. 1. A 2-D linear elastic FGM with an angled edge crack.

For inhomogeneous materials, the more general $\tilde{J}-$integral (Gu et al. 1999) is defined by

$$\tilde{J} = \int_A \left(\sigma_{ij} \frac{\partial u_i}{\partial x_1'} - W\delta_{1j} \right) \frac{\partial q}{\partial x_j'} dA - \int_A \frac{1}{2} \varepsilon_{ij} \frac{\partial D_{ijkl}}{\partial x_1'} \varepsilon_{kl} q dA \tag{6}$$

In order to extract K_I and K_{II} from $J-$integral, the interaction integral which considers two equilibrium states of a cracked body is employed. State 1 is the actual equilibrium state of a body subject to the prescribed boundary conditions while state 2 denotes an auxiliary equilibrium state which will be chosen as the asymptotic fields for modes I or II. In addition, another equilibrium state, called state S, can be led by superposing these two states, for which the $\tilde{J}-$integral in Eq. (6) can be written as (Rao and Rahman 2000)

$$\widetilde{J}^{(S)}=\int_A\left(\left(\sigma_{ij}^{(1)}+\sigma_{ij}^{(2)}\right)\frac{\partial\left(u_i^{(1)}+u_i^{(2)}\right)}{\partial x_1'}-W^{(S)}\delta_{1j}\right)\frac{\partial q}{\partial x_j'}dA+\int_A\frac{\partial}{\partial x_j'}\left(\left(\sigma_{ij}^{(1)}+\sigma_{ij}^{(2)}\right)\frac{\partial\left(u_i^{(1)}+u_i^{(2)}\right)}{\partial x_1'}-W^{(S)}\delta_{1j}\right)qdA \quad (7)$$

with $W^{(S)}=\left(\sigma_{ij}^{(1)}+\sigma_{ij}^{(2)}\right)\left(\varepsilon_{ij}^{(1)}+\varepsilon_{ij}^{(2)}\right)/2=W^{(1)}+W^{(2)}+W^{(1,2)}$.

By utilizing the equilibrium (1) and the compatibility (4), Eq. (7) can be further simplified as

$$\begin{aligned}\widetilde{J}^{(S)}&=\int_A\left(\left(\sigma_{ij}^{(1)}+\sigma_{ij}^{(2)}\right)\frac{\partial\left(u_i^{(1)}+u_i^{(2)}\right)}{\partial x_1'}-\left(W^{(1)}+W^{(2)}+W^{(1,2)}\right)\delta_{1j}\right)\frac{\partial q}{\partial x_j'}dA\\&+\int_A\frac{1}{2}\left(-\varepsilon_{ij}^{(1)}\frac{\partial D_{ijkl}}{\partial x_1'}\varepsilon_{kl}^{(1)}+\sigma_{ij}^{(1)}\frac{\partial\varepsilon_{ij}^{(2)}}{\partial x_1'}-\frac{\partial\sigma_{ij}^{(2)}}{\partial x_1'}\varepsilon_{ij}^{(1)}+\sigma_{ij}^{(2)}\frac{\partial\varepsilon_{ij}^{(1)}}{\partial x_1'}-\frac{\partial\sigma_{ij}^{(1)}}{\partial x_1'}\varepsilon_{ij}^{(2)}\right)qdA\\&=\widetilde{J}^{(1)}+\widetilde{J}^{(2)}+\widetilde{M}^{(1,2)}\end{aligned} \quad (8)$$

Here

$$\widetilde{J}^{(1)}=\int_A\left(\sigma_{ij}^{(1)}\frac{\partial u_i^{(1)}}{\partial x_1'}-W^{(1)}\delta_{1j}\right)\frac{\partial q}{\partial x_j'}dA-\frac{1}{2}\int_A\varepsilon_{ij}^{(1)}\frac{\partial D_{ijkl}}{\partial x_1'}\varepsilon_{kl}^{(1)}qdA \quad (9)$$

$$\widetilde{J}^{(2)}=\int_A\left(\sigma_{ij}^{(2)}\frac{\partial u_i^{(2)}}{\partial x_1'}-W^{(2)}\delta_{1j}\right)\frac{\partial q}{\partial x_j'}dA \quad (10)$$

are two $\widetilde{J}$ – integrals for states 1 and 2, respectively, and

$$\widetilde{M}^{(1,2)}=\int_A\left(\sigma_{ij}^{(1)}\frac{\partial u_i^{(2)}}{\partial x_1'}+\sigma_{ij}^{(2)}\frac{\partial u_i^{(1)}}{\partial x_1'}-W^{(1,2)}\delta_{1j}\right)\frac{\partial q}{\partial x_j'}dA+\int_A\frac{1}{2}\left(\sigma_{ij}^{(1)}\frac{\partial\varepsilon_{ij}^{(2)}}{\partial x_1'}-\frac{\partial\sigma_{ij}^{(2)}}{\partial x_1'}\varepsilon_{ij}^{(1)}+\sigma_{ij}^{(2)}\frac{\partial\varepsilon_{ij}^{(1)}}{\partial x_1'}-\frac{\partial\sigma_{ij}^{(1)}}{\partial x_1'}\varepsilon_{ij}^{(2)}\right)qdA \quad (11)$$

is the modified interaction integral. All the quantities in Eq. (11) are evaluated with respect to a coordinate system originated at the crack tip, and the construction of the integral domain A and the weighting function $q(\boldsymbol{x})$ will be described later.

According to Irwin's relation (1957), the $\widetilde{J}$ – integrals for linear elastic solids under mixed modes I and II also represents the energy release rate. Hence, we have

$$\widetilde{J}^{(1)}=\frac{1}{\overline{E}_{tip}}\left(K_I^{(1)^2}+K_{II}^{(1)^2}\right),\ \widetilde{J}^{(2)}=\frac{1}{\overline{E}_{tip}}\left(K_I^{(2)^2}+K_{II}^{(2)^2}\right) \quad (12)$$

and

$$\widetilde{J}^{(S)}=\widetilde{J}^{(1)}+\widetilde{J}^{(2)}+\frac{2}{\overline{E}_{tip}}\left(K_I^{(1)}K_I^{(2)}+K_{II}^{(1)}K_{II}^{(2)}\right) \quad (13)$$

with $\overline{E}_{tip}=E_{tip}$ for plane stress $\overline{E}_{tip}=E_{tip}/\left(1-\nu^2\right)$ at the crack tip. Equating Eq. (8) and Eq. (13) leads to the following relation give by

$$\widetilde{M}^{(1,2)}=\frac{2}{\overline{E}_{tip}}\left(K_I^{(1)}K_I^{(2)}+K_{II}^{(1)}K_{II}^{(2)}\right) \quad (14)$$

Referring to Anderson (1991), the closed form near-tip displacement fields for modes I

and II in two-dimensional linear fracture mechanics are available. And, the mode I stress intensity factor $K_I^{(1)}$ for state 1 can be determined by making state 2 as the pure mode I asymptotic field (i.e., $K_I^{(2)}=1$ and $K_{II}^{(2)}=0$):

$$\tilde{M}^{(1,Mode\,I)}=\frac{2}{\bar{E}_{tip}}K_I^{(1)} \tag{15}$$

3. NUMERICAL IMPLEMENTATION BY PG-NE METHOD

The boundary value problem of 2-D linear elasticity in the strong form is converted to the weak form according to the usual virtual work principle: Find $\boldsymbol{u}(\boldsymbol{x})$ such that

$$\int_\Omega \boldsymbol{\varepsilon}(\boldsymbol{v}):\boldsymbol{\sigma}(\boldsymbol{u})dv=\int_\Omega \boldsymbol{b}\cdot\boldsymbol{v}\,dv+\int_{\Gamma_N}\hat{\boldsymbol{t}}\cdot\boldsymbol{v}\,ds \tag{16}$$

for every admissible displacement field $\boldsymbol{v}(\boldsymbol{x})$ in the grid-oriented Cartesian coordinate system $\{O,x,y\}$. In order for the Petrov-Galerkin natural element approximation using a given non-convex natural element grid $\Im_{NEM}$ composed of N grid points and Delaunay triangles as shown in Fig. 2(a), trial and test displacement fields $\boldsymbol{u}(\boldsymbol{x})$ and $\boldsymbol{v}(\boldsymbol{x})$ are expanded as

$$\boldsymbol{u}_h(\boldsymbol{x})=\sum_{J=1}^{N}\boldsymbol{u}_J\phi_J(\boldsymbol{x})=\boldsymbol{\Phi}\bar{\boldsymbol{u}}\,,\quad \boldsymbol{v}_h(\boldsymbol{x})=\sum_{I=1}^{N}\boldsymbol{v}_I\psi_I(\boldsymbol{x})=\boldsymbol{\Psi}\bar{\boldsymbol{v}} \tag{17}$$

with Laplace interpolation functions $\phi_J(\boldsymbol{x})$ shown in Fig. 2(b) and CS-FE basis functions $\psi_I(\boldsymbol{x})$. The reader may refer to the references (Cho and Lee, 2006) for more details on the CS-FE basis function defined on three-node trangular elements and the definition of Laplace interpolation fuctions. Meanwhile, Φ and Ψ denote $(2\times 2N)$ matrices containing N basis functions ϕ_J and ψ_I, and $\bar{\boldsymbol{u}}$ and $\bar{\boldsymbol{v}}$ are the $(2N\times 1)$ nodal vectors, respectively.

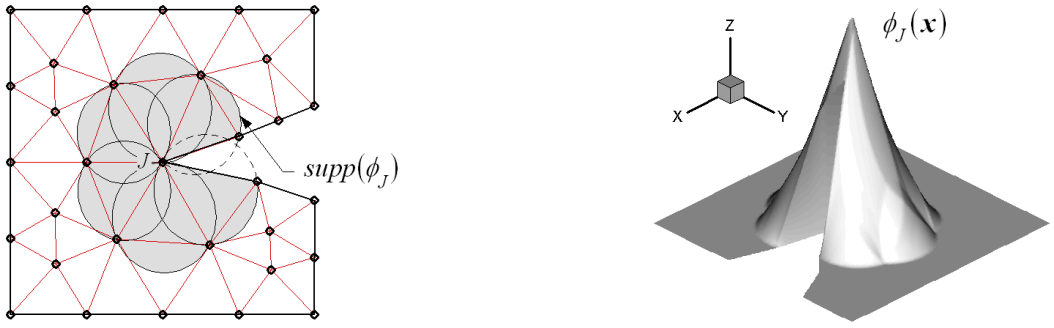

(a) (b)

Fig. 2. (a) Non-convex NEM grid $\Im_{NEM}$, (b) Laplace interpolation function $\phi_J(\boldsymbol{x})$

Substituting Eq. (17) into Eq. (16) leads to the simultaneous linear equations in matrix form given by

$$[\boldsymbol{K}]\bar{\boldsymbol{u}} = \{\boldsymbol{F}\} \tag{18}$$

Here, the global stiffness matrix $[\boldsymbol{K}]$ and the global load vector $\{\boldsymbol{F}\}$ are constructed as following

$$[\boldsymbol{K}] = \sum_{I=1}^{N} \boldsymbol{K}_I, \quad \{\boldsymbol{F}\} = \sum_{I=1}^{N} \boldsymbol{F}_I \tag{19}$$

with the node-wise stiffness matrices and load vectors defined by

$$\boldsymbol{K}_I = \int_{\Omega_v^I} (\boldsymbol{L}\Psi)^T \boldsymbol{E} (\boldsymbol{L}\Phi) dv \tag{20}$$

$$\boldsymbol{F}_I = \int_{\Omega_v^I} \Psi^T \boldsymbol{b}\, dv + \int_{\Gamma_N \cap \Omega_v^I} \Psi^T \hat{\boldsymbol{t}}\, ds \tag{21}$$

Here, $\Omega_v^I = supp(\psi_I(\boldsymbol{x}))$ indicates the support of *I*-th CS-FE basis function and $\boldsymbol{E}$ indicates the (3×3) material constant matrix of linear elasticity. It is noted that the numerical integration in the natural element method is carried out Delaunay triangle by Delaunay triangle.

The weighting function $q(\boldsymbol{x})$ introduced in Eq. (11) should be sufficiently smooth such that its differentiation in the interaction integral (14) is integrable. In the current study, Laplace interpolation function $\phi_J(\boldsymbol{x})$ depicted in Fig. 2(b) which is also used for the trial function is used. Meanwhile, the crack-tip integral domain A is chosen by specifying its radius r_{int} as represented in Fig. 3. The value of unity is assigned to all the nodes within the circle, while the value of zero is specified to the remaining nodes within a whole NEM grid. Then, from the linearity property of Laplace interpolation function (Cho et al., 2013), a darkened rectangular region has the value of unity and its boundary serves as an interior path Γ shown in the previous Fig. 1. Meanwhile, another union of grayed Delaunay triangles have the value $0 \le q \le 1$ and its boundary becomes the outer path Γ_o. In other words, the union of grayed Delaunay triangles automatically becomes the integral domain A.

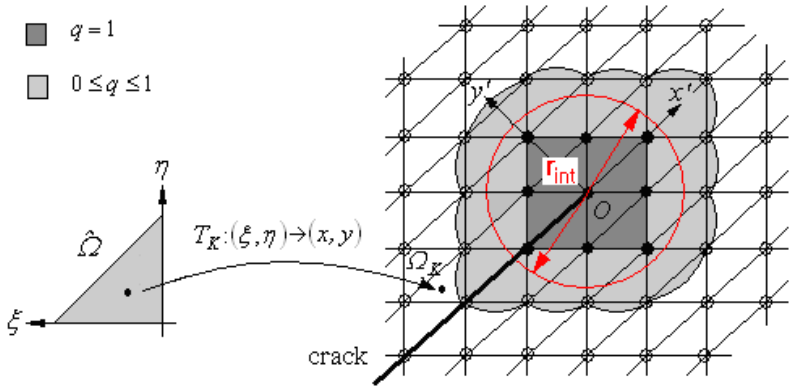

Fig. 3. The construction of the integral domain A and the weighting function $q(\boldsymbol{x})$

Let us denote M_A be the total number of grayed Delaunay triangles within the

integral domain A, then the modified interaction integral (14) is integrated triangle by triangle such that

$$\tilde{M}^{(1,2)} = \sum_{K=1}^{M_A} \tilde{M}_K^{(1,2)} \tag{2}$$

with $\tilde{M}_K^{(1,2)}$ being the triangle-wise interaction integrals. It is because the gradient of weighting function $\partial q / \partial x_j'$ vanishes outside the integral domain A. Here, each triangle-wise interaction integral is computed by

$$\begin{aligned}\tilde{M}_e^{(1,2)} = \sum_{\ell=1}^{INT} \Bigg\{ & \left(\left[\sigma_{ij}^{(1)} \frac{\partial u_i^{(2)}}{\partial x_1'} + \sigma_{ij}^{(2)} \frac{\partial u_i^{(1)}}{\partial x_1'} - W^{(1,2)} \delta_{1j} \right]_{x_\ell} \left. \frac{\partial q}{\partial x_j'} \right|_{x_\ell} w_\ell |J|_{x_\ell} \right. \\ & \left. + \left[\sigma_{ij}^{(1)} \frac{\partial \varepsilon_{ij}^{(2)}}{\partial x_1'} - \frac{\partial \sigma_{ij}^{(2)}}{\partial x_1'} \varepsilon_{ij}^{(1)} + \sigma_{ij}^{(2)} \frac{\partial \varepsilon_{ij}^{(1)}}{\partial x_1'} - \frac{\partial \sigma_{ij}^{(1)}}{\partial x_1'} \varepsilon_{ij}^{(2)} \right] q(x_\ell) w_\ell |J|_{x_\ell} \Bigg\}\end{aligned} \tag{23}$$

using the chain rule and Gauss quadrature rule, in which INT, $\boldsymbol{x}_\ell$ and w_ℓ indicate the total number of integration points, sampling points and weights, respectively. Note that the sampling points $\boldsymbol{x}_\ell$ in Ω_K and the Jacobian $|\boldsymbol{J}|_{\boldsymbol{x}_\ell}$ are calculated using the geometry transformation T_K defined by

$$T_K : x_\ell = \sum_{i=1}^{3} x_i \psi_i(\xi,\eta)_\ell, \quad y_\ell = \sum_{i=1}^{3} y_i \psi_i(\xi,\eta)_\ell \tag{24}$$

between Ω_K in NEM grid and the master triangle element $\hat{\Omega}$. Here, $\{x_i, y_i\}$ are the co-ordinates of three nodes in each Delaunay triangle, $(\xi,\eta)_\ell$ the Gauss points in $\hat{\Omega}$, and ψ_i the triangular shape functions.

4. NUMERICAL EXPERIMENT

We consider a slant edge crack in a 2-D FGM plate in plane stress condition with the height $H = 2$ units and the width $W = 1$ unit. Referring to Fig. 4(a), the crack angle α is 45^o and the relative crack length is $a/W = 0.4\sqrt{2}$. The Poison's ratio is kept constant with $\nu = 0.3$, but the elastic modulus is assumed to be an exponential function in the $x-$direction, given by

$$E(x) = \bar{E}\, exp[\eta(x - 0.5)], \quad 0 \le x \le W \tag{25}$$

Where, $\bar{E} = 1$ unit and ηa is variable for the parametric study such as $\eta a = 0, 0.1, 0.25, 0.5, 0.75$ and 1.0. As external load, an exponentially varying distributed load is applied to the upper edge with $\sigma_{yy}(x,1) = \bar{\varepsilon}\bar{E}\, exp[\eta(x - 0.5)]$ with $\bar{\varepsilon}$ being 1. All the bottom edge is constrained in the vertical direction (i.e., $u_y = 0$), and in addition the right end is constrained in the horizontal direction at the same time. A locally refined NEM grid shown in Fig. 4(b) is used, which is uniformly discretized by 10×20 and the near-tip

region is locally refined with eight additional grid points. The total number of grid points is 244 because five additional grid points are needed to split a crack line into upper and lower lines. All the numerical integrations for the NEM analysis, the patch recovery and the modified interaction integral were performed using 13 Gassian points.

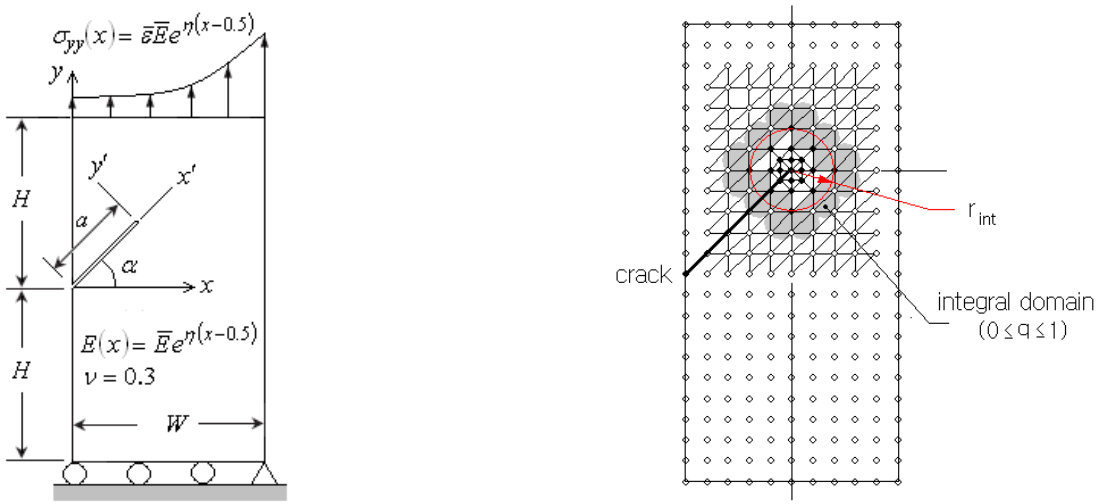

(a) (b)

Fig. 4. (a) A FGM plate with a slant edge crack under the exponentially varying distributed load, (b) a locally refined NEM grid and the integral domain (244 nodes).

Table 1 comparatively represents the predicted normalized SIFs $K_I / \bar{\varepsilon}\bar{E}\sqrt{\pi a}$ and $K_{II} / \bar{\varepsilon}\bar{E}\sqrt{\pi a}$ obtained for seven different ηa values. For the comparison purpose, the numerical results by Kim and Paulino (2002) and Rao and Rahman (2003) are also presented. It is noted that the FEM results by Kim and Paulino were obtained by the path-independent J_k^* – integral approach while the EFGM (element-free Galerkin method) results by Rao and Rahman were by the modified interaction integral $\tilde{M}^{(1,2)}$. It is observed that the proposed method is in good agreement with FEM and EFGM such that the maximum relative difference is 4.01% at $K_{II} / \bar{\varepsilon}\bar{E}\sqrt{\pi a}$ for $\eta a = 0.25$. Meanwhile, it is found that the present method provides slightly lower SIFs than FEM and EFGM at low ηa but the present method predicts slightly higher SIFs at high ηa.

Table 1 Normalized SIFs for a slanted crack in a functionally graded plate

ηa	Proposed method		Kim and Paulino [J_k^*]		Rao and Rahman [$\tilde{M}^{(1,2)}$]	
	$\frac{K_I}{\bar{\varepsilon}\bar{E}\sqrt{\pi a}}$	$\frac{K_{II}}{\bar{\varepsilon}\bar{E}\sqrt{\pi a}}$	$\frac{K_I}{\bar{\varepsilon}\bar{E}\sqrt{\pi a}}$	$\frac{K_{II}}{\bar{\varepsilon}\bar{E}\sqrt{\pi a}}$	$\frac{K_I}{\bar{\varepsilon}\bar{E}\sqrt{\pi a}}$	$\frac{K_{II}}{\bar{\varepsilon}\bar{E}\sqrt{\pi a}}$
0.0	1.430	0.599	1.451	0.604	1.448	0.610
0.1	1.376	0.577	1.396	0.579	1.391	0.585
0.25	1.302	0.527	1.316	0.544	1.312	0.549
0.5	1.189	0.482	1.196	0.491	1.190	0.495
0.75	1.088	0.447	1.089	0.443	1.082	0.446
1.0	0.999	0.413	0.993	0.402	0.986	0.404

CONCLUSION

A slant edge crack for evaluating mixed-mode SIFs was parametrically investigated in order to illustrate and validate the proposed method. The elastic modulus was assumed to be an exponential function and the corresponding index was taken as a parametric variable. The predicted SIFs obtained by the proposed method were compared with the other numerical results. From the comparison, the prediction accuracy of the proposed method has been verified such that the maximum relative difference is less than 5%. Thus, it has been confirmed that the proposed method is correlated satisfactorily with the J_k^* – integral using FEM and the modified interaction integral $\left[\tilde{M}^{(1,2)}\right]$ using EFGM.

ACKNOWLEDGEMENT

This research was supported by Basic Science Research Program through the National Research Foundation of Korea (NRF) funded by the Ministry of Education (Grant No. NRF-2017R1D1A103028879).

REFERENCES

Anderson, T.L. (1991) *Fracture Mechanics: Fundamentals and Applications*, 1st edition, CRC Press.

Anlas, G., Santare, M.H. and Lambros, J. (2000) “Numerical calculation of stress intensity factors in functionally graded materials”, *Int. J. Fracture*, **104**, 131-143.

Apalak, M.K. (2014) “Functionally graded adhesively bonded joints”, *Rev. Adhesion Adhesive*., **1**, 56-84.

Atkinson, C. and List, R.D. (1978) “Steady state crack propagation into media with spatially varying elastic properties”, *Int. J. Eng. Sci*., **16**, 717-730.

Cho, J.R. and Lee, H.W. (2006) “A Petrov-Galerkin natural element method securing the numerical integration accuracy”, *J. Mech. Sci. Technol*., **20**(1), 94-109.

Cho, J.R., Lee, H.W. and Yoo, W.S. (2013) “Natural element approximation of Reissner-Mindlin plate for locking free numerical analysis of plate-like thin elastic structures”, *Comput. Meth. Appl. Mech. Engrg*., **256**, 17-28.

Cho, J.R. (2016) “Stress recovery techniques for natural element method in 2-D solid mechanics”, *J. Mech. Sci. Technol.,* **30**(11), 5083-5091.

Delale, F. and Erdogan, F. (1983) “The crack problem for a nonhomogeneous plane”, *J. Appl. Mech*., **50**, 609-614.

Dhaliwal, R.S. and Singh, B.M. (1978) “On the theory of elasticity of a nonhomogeneous medium”, *Int. J. Elasticity*, **8**, 211-219.

Dolbow, J.E. and Gosz, M. (2002) “On the computation of mixed-mode stress intensity factors in functionally graded materials”, *Int. J. Solids Struct*., **39**(9), 2557-2574.

Giannakopulos, A.E., Suresh, S., Olsson, M. (1995) “Elastoplastic analysis of thermal cycling: layered materials with compositional gradients”, *Acta Metall. Mater*., **43** (4), 1335-1354.

Gu, P., Dao, M. and Asaro, R.J. (1999) “A simplified method for calculating the crack tip field of functionally graded materials using the domain integral”, *J. Appl. Mech*., **66**(1), 101-108.

Irwin, G.R. (1957) “Analysis of stresses and strains near the end of a crack traveling a plate”, *J. Appl. Mech*., **24**, 361-364.

Kawasaki, K. and Watanabe, R. (2002) “Thermal fracture behavior of metal/ceramic functionally graded materials”, *Eng. Fracture Mech.,* **69**(14-16), 1713-1728.

Kim, J.H. and Paulino, G.H. (2002) “Finite element evaluation of mixed mode stress intensity factors in functionally graded materials”, *Int. J. Numer. Methods Engng*., **53**, 1903-1935.

Miyamoto, Y., Kaysser, W.A., Rabin, B.H. and Kawasaki, A. (2013) *Functionally Graded Materials: Design. Processing and Applications*, Springer Science & Business Media.

Rao, B.N. and Rahman, S. (2000) “An efficient meshless method for fracture analysis of cracks”, *Comput. Mech.,* **26**, 398-408.

Rao, B.N. and Rahman, S. (2003) “Mesh-free analysis of cracks in isotropic functionally graded materials”, *Eng. Fracture Mech*., **70**, 1-27.

Tilbrook, M.T., Moon, R.J. and Hoffman, M. (2005) “Crack propagation in graded composites”, *Composite Sci. Technol*., **65**(2), 201-220.

Vel, S.S. and Goupee, A.J. (2010) “Multiscale thermoelastic analysis of random heterogeneous materials, Part I: microstructure characterization and homogenization of material properties”, *Comput. Mater. Sci*., **48**, 22-38.

Zhang, Ch., Sladek, J. and Sladek, V. (2004) “Crack analysis in unidirectionally and bidirectionally functionally graded materials”, *Int. J. Fracture*, **129**, 385-406.